Theoretical and experimental study of the structural, dynamical and dielectric properties of perovskite $BaSnO_3$

2008 J. Phys.: Condens. Matter 20 145217

(http://iopscience.iop.org/0953-8984/20/14/145217)

J. Phys.: Condens. Matter **20** (2008) 145217 (6pp) doi:10.1088/0953-8984/20/14/145217

Theoretical and experimental study of the structural, dynamical and dielectric properties of perovskite $BaSnO_3$

Émile Bévillon, Anthony Chesnaud, Yanzhong Wang, Guilhem Dezanneau and Grégory Geneste

Laboratoire Structure, Propriétés et Modélisation des Solides, UMR CNRS 8580, Ecole Centrale Paris, Grande Voie des Vignes, 92295 Chatenay-Malabry Cedex, France

Received 9 January 2008, in final form 17 February 2008
Published 19 March 2008
Online at stacks.iop.org/JPhysCM/20/145217

Abstract

The structural, dynamical and dielectric properties of the cubic phase of perovskite barium stannate $BaSnO_3$, a potential candidate as protonic conductor for solid oxide fuel cells, have been investigated by the means of first-principles density functional calculations, and the structural and electrical properties have been explored at low temperature. From density functional perturbative calculations, the phonon modes, the Born effective charges and the dielectric tensor are derived and analyzed, at zero pressure. The phonon band-structure of the cubic phase does not exhibit unstable modes, in good agreement with x-ray diffraction, which shows that $BaSnO_3$ remains perfectly cubic down to 10 K. The dielectric response in $BaSnO_3$ as measured and calculated is lower than in titanate and zirconate perovskites.

1. Introduction

Perovskite stannates $ASnO_3$ (A = Ca, Sr or Ba) are an interesting group of materials that may exhibit structural deviations from the ideal perovskite: $CaSnO_3$ and $SrSnO_3$ have an orthorhombic structure (space group $Pnma$—$a^-b^+a^-$ in Glazer notation) whereas $BaSnO_3$ is known to be cubic (space group $Pm\bar{3}m$) at room temperature. This compound has recently been proposed as a protonic conductor [1–3] with potential applications in fuel cells, when Sn is partially substituted by trivalent metals (Y [2], In [3]) and activated by reaction with ambient moisture. With such dopants, interesting levels of hydration and protonic conduction have been measured. Other applications in gas sensors are proposed for this compound [4, 5]. Partial substitution by other metals on the A or B site have been reported (Cr, La [6], Ce, Nd [7]). Moreover, $BaSnO_3$ have also been suggested to have promising potentialities in photoelectrochemical applications [8, 9], since its band gap (≈3.4 eV) is similar to the gap of the best known hydrogen photocatalysts (TiO_2, $SrTiO_3$, ZnO, etc). At high hydrostatic pressure, an interesting dielectric behavior is also predicted [10].

Despite the interest in $BaSnO_3$ in the field of hydrogen technology, there are, to our knowledge, few experimental and theoretical studies on this compound: the electronic structure of $BaSnO_3$ was investigated 15 years ago by Singh *et al* [11], and some interatomic potentials for perovskite stannates, available to describe their structure and defect formation energies, have been provided [12]. Therefore, we have investigated a number of properties of this compound within first-principles density functional calculations. X-ray diffraction and dielectrical measurements have been performed down to low temperature to test the prediction of theory.

The aim of this paper is (1) to provide experimental and theoretical results for a better understanding of the physical properties, especially those which can be determining in the protonic transport (vibrations, polarizability, dielectric response, etc), and (2) to examine the possibility of structural distortions in this compound at low temperature.

$BaSnO_3$ is known to be perfectly cubic at room temperature and ambient pressure [13]. Its Goldschmidt tolerance factor, $t = (r_A + r_O)/\sqrt{2}(r_B + r_O) = 1.02$ according to Shannon's ionic radii [14], is indeed probably too low to allow polar distortions and probably too high to allow octahedral tilts. Anyway, other perovskite stannates with smaller cations on the A site, and thus lower tolerance factors, such as $SrSnO_3$ and $CaSnO_3$, exhibit structural distortions related to antiferrodistortive motions of the oxygen octahedra. $SrSnO_3$ (orthorhombic—space group $Pnma$ at RT [15, 16]) even presents a complex succession of phase transitions with

temperature [17]. Barium stannate has a tolerance factor very close to that of $BaZrO_3$, a compound which has recently attracted interest [18, 19] concerning its structure since an antiferrodistortion is predicted by DFT but not observed. To our knowledge, the possibility of such instabilities at low temperature has not been investigated in $BaSnO_3$ either within first-principles calculations or within experimental studies.

This work will thus help us to get further insight into the understanding of $BaSnO_3$ and will constitute a basis for the development of doped compounds for hydrogen-related properties such as proton conduction or water photolysis. We also test the presence of instabilities in the phonon band-structure of this material. Theoretical results are in all cases compared to experimental results as given by x-ray diffraction or dielectric measurements. The paper is organized as follows: the experimental procedure and the computational details of the numerical scheme are presented in section 2. Section 3 presents the results related to the structural, dynamical and dielectric properties of the crystal. They are discussed in section 4.

2. Method

2.1. Experimental procedure

$BaSnO_3$ powder has been synthesized by a polymerization route from an aqueous solution containing cation salts. First, a tin solution (with Sn^{2+} content of 0.093 mol L^{-1}) was prepared by dissolving tin metal in diluted nitric acid solution (0.2 mol L^{-1}). In another beaker, 10.45 g of $Ba(NO_3)_2$ was completely dissolved into ultra-pure water, and pH was fixed to 1.0 by addition of few drops of a nitric acid solution (13 mol L^{-1}). Then, the two solutions were mixed, resulting in a clear transparent solution with total volume equal to 600 ml and pH value close to 1.0. This pH value was increased to a value of 6 by adding ammonium hydroxide solution. To this solution was then added 50 ml of acrylic acid followed by 2.8 g of N,N'-methylene bis-acrylamide. The solution is then heated slowly and several droplets of hydrogen peroxide are added. At this moment, two organic compounds react together to form a cross-linked polymer containing the solution. The gel obtained is then dried in a microwave oven to obtain a precursor that is calcined at 1473 K for 4 h to lead to the desired $BaSnO_3$ compounds. No presence of an extra peak, relating to impurity phases, was observed by x-ray diffraction (XRD): a pure and well crystallized sample was obtained. A sintered sample was thus obtained by spark plasma sintering in an SPS Dr Sinter 2080 furnace (Sumitomo Coal Mining). 300–400 mg of powder were directly put into a cylindrical graphite die in order to form final pellets of 8 mm diameter and 1 mm thickness. The die/powder assembly was then introduced into the sintering chamber. We observed that a sintering temperature of 1423 K was sufficient to obtain good density. Nevertheless, argon atmosphere was necessary (instead of vacuum) to avoid tin reduction. The sintering process is as follows: the pressure and temperature are progressively increased till their maximum (100 MPa and 1423 K), maintained for 3 min and then they are released. Once the sintering process is finished, a final thermal treatment of several hundred degrees is generally necessary to eliminate carbon pollution from the graphite die.

The x-ray powder diffraction (XRPD) pattern of the pellet was recorded on a high accuracy two-axis diffractometer, in a Bragg–Brentano geometry, using Cu Kα_1 radiation as x-ray source which was generated by a 18 kW rotating anode. The data were collected, in the 2θ region between 10° and 130°, with a 0.03° angular step. These experiments were performed respectively in a helium cryostat from 7 to 298 K (RT) and in a furnace under vacuum for the range RT–773 K. The evolution of the cubic cell parameter was determined out using the program DiffracPlus Topas from Bruker AXS. Electrical measurements were performed on home-made jig inside a helium cryostat. In this case, the two sides of the pellet were painted by platinum ink further heat-treated at 1273 K for 2 h. The dielectric constant was measured at 10 kHz in a two-point configuration using an HP 4294A impedancemeter. In this case, the sample cooled down to 10 K in a helium cryostat was allowed to warm slowly till room temperature, while temperature and impedance were measured every 10°.

2.2. Computational details

The calculations are performed in the framework of the density functional theory (DFT) [20] within the ABINIT code[1]. Most of the calculations are performed using the generalized gradient approximation (GGA) to model the exchange and correlation energy, in the form proposed by Perdew, Burke and Ernzerhof (PBE) [22]. The effect of core electrons is accounted for through the use of Troullier–Martins pseudopotentials [23], generated within the FHI98PP code [24]. The pseudopotential for Ba takes into account the $5s^2$, $5p^6$ and $6s^2$ electrons in the valence and is generated from an ionic reference configuration Ba^{2+} ($5s^2$, $5p^6$ and $6s^0$). For Sn the four electrons $5s^2$ and $5p^2$ are taken in the valence, and for O the $2s^2$ and $2p^4$ electrons are treated. The results obtained on the structural parameters of the corresponding binary oxides (BaO and SnO_2) are reported in table 1. In a number of cases, the results obtained have been checked by using a more complex Sn pseudopotential that also includes the 4d electrons in the valence. The explicit treatment of these electronic levels may be important to describe some properties of the compound. Also, the local density approximation (LDA), through the parametrization of Perdew and Wang (PW92) [25], has been used in some cases for comparison.

We use a $6 \times 6 \times 6$ Monkhorst–Pack mesh to sample the first Brillouin zone (FBZ) of the five-atom ABO_3 unit cell. Indeed, the lattice parameter of $BaSnO_3$ is perfectly converged when changing the mesh from a $4\times4\times4$ to a $6\times6\times6$ one. The periodic parts of the Kohn–Sham wavefunctions are expanded on a plane wave basis set with a 30 Hartree cut-off, for which the lattice constants of BaO, SnO_2 and $BaSnO_3$ are found to be perfectly converged. For the sake of numerical accuracy, the linear response calculations are performed at a 50 Hartree cut-off.

[1] The ABINIT code is a common project of the Université Catholique de Louvain, Corning Incorporated, and other contributors (URL: http://www.abinit.org [21]).

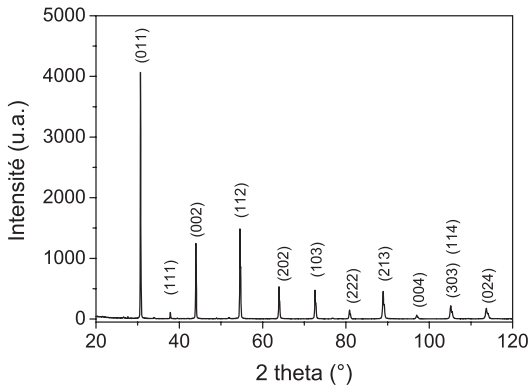

Figure 1. X-ray diffraction diagram of $BaSnO_3$ at $T = 10$ K.

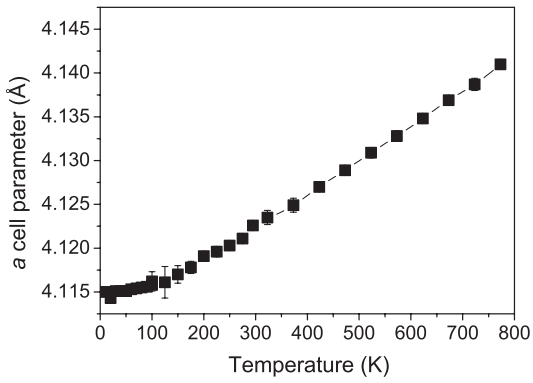

Figure 2. $BaSnO_3$ cell parameter evolution with respect to temperature.

Table 1. Structural results obtained in the present study for BaO, SnO_2 and $BaSnO_3$. The results on $BaSnO_3$ are obtained assuming a cubic $Pm\bar{3}m$ structure.

Solid	Structure	*a* (Å)	*c* (Å)	Internal parameter	Method
BaO	Rock-salt	5.586	—	—	GGA-PBE
		5.52	—	—	Expt
SnO_2	Rutile	4.794	3.207	0.3065	GGA-PBE
		4.737	3.188	0.307	Expt
$BaSnO_3$	Perovskite	4.156	—	—	GGA-PBE Sn: no semicore
		4.186	—	—	GGA-PBE Sn: 4d semicore
		4.116	—	—	Expt

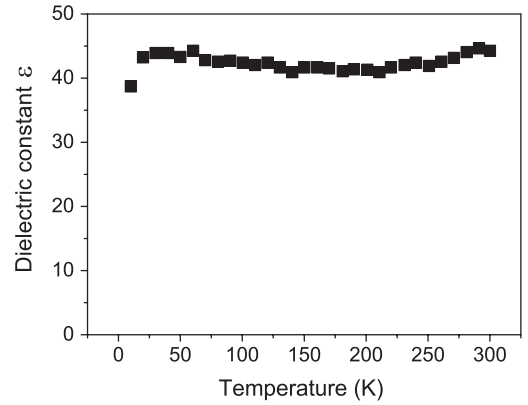

Figure 3. Temperature evolution of the dielectric constant of $BaSnO_3$.

Two kinds of calculations have been performed: first, total energy calculations and structural optimization of the five-atom unit cell within the BFGS algorithm implemented in the ABINIT code; then perturbative density functional calculations (DFPT), giving access to (1) the Born effective charges, which are known to reach very large values in perovskites presenting polar structural instabilities, (2) the optic dielectric tensor, and (3) the phonon spectrum on the whole Brillouin zone, including the LO–TO splitting at Γ. From all these results the static dielectric tensor is also computed.

The static (topological) charges are estimated using the Bader method [26].

3. Results

3.1. Experimental results

X-ray diffraction experiments have been performed down to 10 K. In figure 1, we present the x-ray diffraction diagram of the pellet sample obtained at 10 K. We also show in this figure the indexation of the peaks considering a cubic structure with $Pm\bar{3}m$ space group. The results show then that even at low temperature the $BaSnO_3$ compound does not present any transition to a lower symmetry structure, keeping its high symmetry cubic structure. Nevertheless, some very small additional peaks are observed at 2θ angles of 26.8°, 34.0° and 52.0°, which are attributed to the SnO_2 cassiterite phase. This may reflect some small loss of barium during sintering. The very thin peak at 27.9° is due to a Kβ contribution not totally eliminated by the graphite monochromator.

The temperature evolution of the lattice parameter is shown in figure 2 and the measured thermal expansion coefficient is 9.6×10^{-6} K^{-1}.

The dielectric constant measured at 10 kHz is represented in figure 3 as a function of temperature. There is no significant evolution of this value, which gives another confirmation that no structural change occurs in this compound. The observed value around 40 is significantly higher than the one calculated from *ab initio* computations (see hereafter). This may come from experimental errors, in spite of the calibration procedure, since measurements are easily biased by impurity contributions for such low dielectric constant values. This is all the more probable in this case as the jig was essentially built for measuring high dielectric constant materials.

We stress that in some cases weak oxygen octahedral tilts, that would be coupled with a very low strain, are difficult to detect within x-ray diffraction. Anyway, the evolution of the cell parameter with temperature does not exhibit peaks or discontinuities, consistent with the absence of a phase transition. Moreover, the DFT calculations (see hereafter) do not reveal the existence of unstable modes in the phonon band-structure of $BaSnO_3$. Thus we conclude that this compound probably remains cubic down to 0 K.

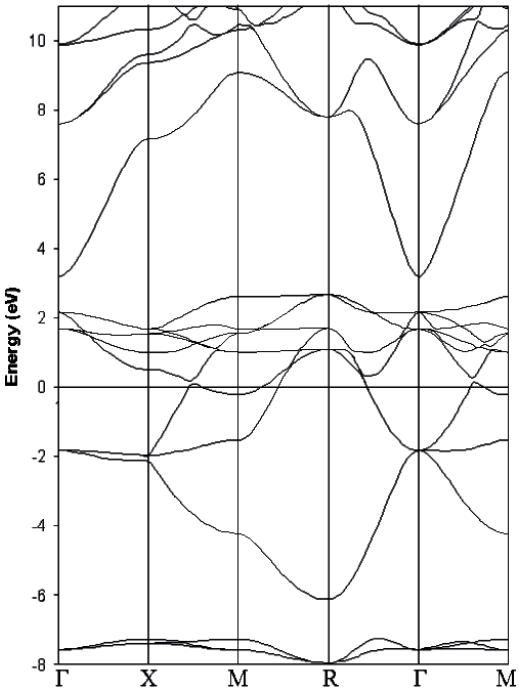

Figure 4. Electronic band-structure of $BaSnO_3$ along the line Γ–X–M–R–Γ–M. Energies are in eV.

3.2. DFT calculations

3.2.1. Lattice parameter and elastic constants in the cubic structure $Pm\bar{3}m$. After structural optimization in the cubic symmetry (space group $Pm\bar{3}m$), the lattice parameter of $BaSnO_3$ is found to be 4.156 Å in GGA, in very good agreement with the experimental value (4.116 Å at room temperature). This small overestimation ($\approx 1\%$) is typical of the GGA. The explicit treatment of the 4d semicore levels of Sn yields an equilibrium lattice constant of 4.186 Å.

The Young modulus (E) and Poisson coefficient (ν) have been computed by setting the cell parameter along the z axis at different fixed values (corresponding both to tensile and compressive stress) and performing full stress relaxation in the perpendicular directions. For a given strain imposed along z (ϵ_{zz}), one gets after full optimization a stress component along z (σ_{zz}) and a strain in the lateral directions x and y (ϵ_{xx} and ϵ_{yy}). E and ν are thus simply evaluated by

$$E = \frac{\sigma_{zz}}{\epsilon_{zz}} \qquad \nu = -\frac{\epsilon_{xx}}{\epsilon_{zz}}. \tag{1}$$

Using the least squares method to fit the results in the linear part of the curve, we find $E = 207$ GPa and $\nu = 0.233$. The shear modulus has been deduced using the following formula, available in isotropic materials:

$$G = \frac{E}{2(1+\nu)}. \tag{2}$$

We find $G = 84$ GPa. The Young modulus and the shear modulus are measured respectively at 244 GPa and 99.9 GPa in [13].

Table 2. Born effective charges and static (topological) charges obtained on $BaSnO_3$ (GGA result). The tensors are diagonal in the axis of the cubic perovskite structure, so only the diagonal terms are given.

	Effectives charges:			
Atom	Z^*_{xx}	Z^*_{yy}	Z^*_{zz}	Topological charges
Ba	2.73	2.73	2.73	1.55
Sn	4.37	4.37	4.37	2.44
O1	−1.87	−1.87	−3.37	−1.33
O2	−1.87	−3.37	−1.87	−1.33
O3	−3.37	−1.87	−1.87	−1.33

3.2.2. Electronic structure and static charges. The electronic band-structure has been computed at the GGA theoretical lattice parameter (4.156 Å), along a path in the FBZ defined by Γ–X–M–R–Γ–M. $BaSnO_3$ is found to be an indirect band gap insulator (gap ≈1.4 eV in GGA), in agreement with Singh *et al* [11], who mention 0.79 and 2.03 eV. Borse *et al* find a lower value (0.3 eV) in GGA [8]. All these values are strongly underestimated with respect to the experimental value (3.4 eV), as usual in DFT ground state calculations. The band-structure and the electronic density of states are shown in figures 4 and 5 respectively. Both are very close to the results of [11] obtained by the LAPW method.

The topological charges [26] are found to be +1.55 for Ba, +2.44 for Sn and −1.33 for O. The static charge of Ba is quite close to its formal charge (+2), reflecting the marked ionic character of the Ba–O bond. In contrast, the Sn static charge differs from its formal value (+4) by more than 1.5 electrons, indicating that the Sn–O bond is strongly ionocovalent.

3.2.3. Born effective charges and dielectric tensor. The Born effective charge $Z^{(i)}_{\alpha\beta}$ is the first derivative of the macroscopic polarization P_α (along the α direction) with respect to the displacement of atom (i) along the β direction. In perfect ionic crystals, this quantity would be close to the static charge obtained through integration of the electronic density around the ion. In ionocovalent crystals such as $BaSnO_3$, it may significantly differ from this value since electron transfers may occur along the ionocovalent bond as the (i) atom is displaced, due to the change in orbital overlap related to the partial covalency of the interatomic bonds. This effect is enhanced in ferroelectric crystals, where effective charges may reach very large values.

The values obtained for the Born effective charges in GGA are listed in table 2. The LDA values are almost the same (differences $\leqslant 0.06e$). The (isotropic) optic dielectric tensor is found to be 4.895 (GGA).

3.2.4. Phonons and static dielectric constant. The phonon dispersion curves have been calculated on the whole Brillouin zone, at the *experimental* lattice constant (figure 6).

There is no ferroelectric instability at Γ, in good agreement with our XRD experiments, which suggest that $BaSnO_3$ is cubic down to low temperature. The tolerance factor in $BaSnO_3$ (=1.02) is moreover not consistent with

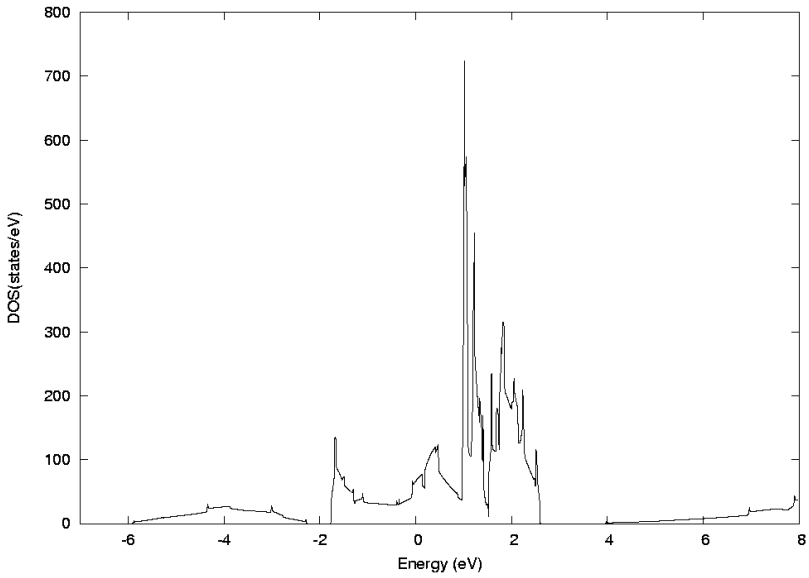

Figure 5. Electronic density of states of $BaSnO_3$.

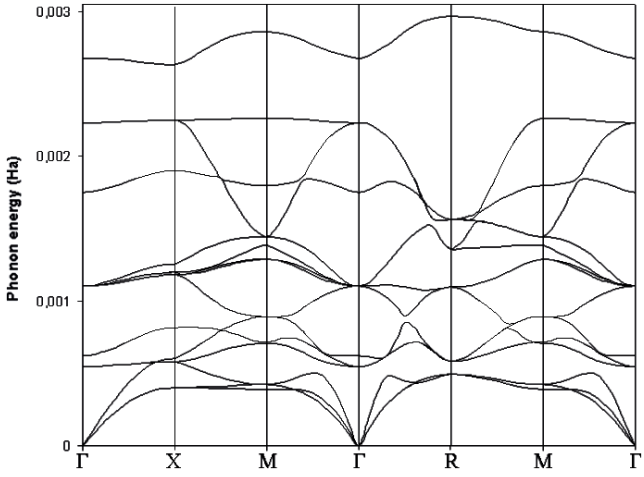

Figure 6. Phonon dispersion curves of $BaSnO_3$, calculated within the LDA at the experimental lattice constant.

the appearance of such an instability (it is usually higher in ferroelectric materials). The eigenfrequencies of the modes at Γ (including LO–TO splitting) as well as their effective charges are given in table 3 for the LDA and the GGA (the transverse optic modes are labeled by TO1, TO2 and TO3).

From the mode effective charges and the optic dielectric tensor, the static dielectric constant can be computed: we find $\epsilon_S = 22.3$ (GGA and LDA). The LDA results are all very close to the GGA ones. We note that the LDA and GGA values of the frequencies and effective charges of TO2 and TO3 differ significantly. In contrast, TO1 has almost the same frequency and effective charge, whether calculated within the LDA or the GGA. This explains why the static dielectric constant, calculated in the harmonic approximation, from

$$\epsilon_{S\alpha\beta} = \epsilon^{\infty}_{\alpha\beta} + \frac{4\pi}{\Omega} \sum_{\text{modes}\tau} \frac{S^{\tau}_{\alpha\beta}}{\omega^2_{\tau}} \tag{3}$$

is found to be the same in LDA and in GGA.

Table 3. Mode effective charges obtained on $BaSnO_3$ for the modes calculated at Γ. Frequencies are in cm^{-1}, and Z^* are in e. Non-zero Z^* correspond to IR-active modes, with Γ_{15} symmetry.

Mode	ω (GGA)	ω (LDA)	Z^* (GGA)	Z^* (LDA)
TO1	121.2	120.3	2.85	2.76
LO1	132.2	136.9	2.85	2.76
Γ_{25}	207.5	242.3	0.00	0.00
TO2	219.7	242.3	3.82	4.32
LO2	355.8	384.9	3.82	4.32
TO3	563.6	490.6	2.99	2.40
LO3	652.1	588.2	2.99	2.40

4. Discussion: crystal structure at low temperature and dielectric response

The crystal structure of $BaSnO_3$ is found to be cubic (space group $Pm\bar{3}m$) down to 10 K, as suggested by our DFT calculations. All the eigenmodes at Γ are found to be stable in the $Pm\bar{3}m$ structure, in agreement with the absence both of polar distortion and antiferrodistortion.

The response function calculations performed on $BaSnO_3$ (dielectric tensor, effective charges) suggest that the dielectric response of barium stannate is lower than that of titanate, zirconate and niobate perovskites. For example, the Born effective charges in $BaTiO_3$, calculated within the LDA by Ghosez *et al* [27], are 7.32 (Ti) and −2.14 and −5.78 (O), much higher than those of Sn and O in $BaSnO_3$. Ba's value anyway (2.74) is very close to ours. The low values we obtain in $BaSnO_3$ for the Born effective charges and for the mode effective charges (in particular, $Z^*(TO1) \approx 2.8$) explain the absence of polar distortion and strong dielectric response. The electronic polarizability is also lower than in $BaTiO_3$ since the (isotropic) optic dielectric tensor is equal to 4.89 in $BaSnO_3$ ($\epsilon^{\infty} = 6.75$ [27] in $BaTiO_3$). In $BaZrO_3$, which is not ferroelectric, the static dielectric constant reaches 45–50 at low temperature [18, 19].

At R in $BaSnO_3$, at the experimental lattice constant, the LDA does not exhibit instabilities. Antiferrodistortive

instabilities are common in perovskite oxides. Their existence is usually related to a low value of the tolerance factor ($t \leqslant 1$) [28]. In other stannates, such instabilities yield lower symmetry structures ($SrSnO_3$: $t = 0.96$, $CaSnO_3$: $t = 0.93$). In $BaZrO_3$, which has exactly $t = 1$, an antiferrodistortion is predicted but not observed [18, 19], probably because of zero-point quantum effects. In $BaSnO_3$, which has $t = 1.02$, there is thus no such driving force to deform the structure, and the crystal is accordingly perfectly cubic even at low temperature.

5. Conclusion

In this paper, the structural, dynamical and dielectric properties of $BaSnO_3$ have been investigated by DFT calculations and x-ray diffraction experiments. This work constitutes the starting point of a wider study of barium stannate as a protonic conductor, which will include (1) doping by trivalent metals and the insertion of water, (2) the diffusion of protons once H_2O dissociates in the oxygen vacancies generated by the doping.

Acknowledgments

The present research was partially funded by the contribution of the 'Agence Nationale pour la Recherche' (ANR), program 'Jeunes chercheuses, jeunes chercheurs', within the project no. JC05-42231. The authors thankfully acknowledge the computer resources, technical expertise and assistance provided by the Barcelona Supercomputing Center—Centro Nacional de Supercomputación. Some of the calculations have been performed thanks to the facilities of the CNRS Supercomputing Center (IDRIS). SPS sintering has been performed by C Estournès at the National Platform for Flash Sintering at the CIRIMAT laboratory of Toulouse (France).

References

[1] Kreuer K D 1999 *Solid State Ion.* **125** 285–302
[2] Murugaraj P, Kreuer K D, He T and Schober T 1997 *J. Mater. Solid State Ion.* **98** 1–6
[3] Schober T 1998 *Solid State Ion.* **109** 1–11
[4] Cerdá J, Arbiol J, Dezanneau G, Diaz R and Morante J R 2002 *Sensors Actuators* B **84** 21–5
[5] Manorama S V, Gopal Reddy C V and Rao V J 2001 *Appl. Surf. Sci.* **174** 93–105
[6] Upadhyay S, Parkash O and Kumar D 2001 *Mater. Lett.* **49** 251–5
[7] James J, Kumar O B S, Senthil Kumar S, Prabhakar Rao P and Nair K V O 2003 *Mater. Lett.* **57** 3641–7
[8] Borse P H, Lee J S and Kim H G 2006 *J. Appl. Phys.* **100** 124915
[9] Yuan Y, Lv J, Jiang X, Li Z, Yu T, Zou Z and Ye J 2007 *Appl. Phys. Lett.* **91** 094107
[10] Bevillon E and Geneste G 2007 *Phys. Rev.* B **75** 214106
[11] Singh D J, Papaconstantopoulos D A, Julien J P and Cyrot-Lackmann F 1991 *Phys. Rev.* B **44** 9519–23
[12] Hines R I, Allan N L and Flavell W R 1996 *Phil. Mag.* B **73** 33–9
[13] Maekawa T, Kurosaki K and Yamanaka S 2006 *J. Alloys Compounds* **416** 214–7
[14] Shannon R D 1976 *Acta Crystallogr.* A **32** 751
[15] Beurmann P S, Thangadurai V and Weppner W 2003 *J. Solid State Chem.* **174** 392–402
[16] Green M A, Prassides K, Day P and Neumann D A 2000 *Int. J. Inorg. Mater.* **2** 35–41
[17] Mountstevens E H, Redfern S A T and Attfield J P 2005 *Phys. Rev.* B **71** 220102(R)
[18] Akbarzadeh A R, Kornev I, Malibert C, Bellaiche L and Kiat J-M 2005 *Phys. Rev.* B **72** 205104
[19] Bennett J W, Grinberg I and Rappe A 2006 *Phys. Rev.* B **73** 180102R
[20] Kohn W and Sham L J 1965 *Phys. Rev.* **140** A1133
[21] See also Gonze X *et al* 2002 *Comput. Mater. Sci.* **25** 478–92
[22] Perdew J P, Burke K and Ernzerhof M 1996 *Phys. Rev. Lett.* **77** 3865
[23] Troullier N and Martins J L 1991 *Phys. Rev.* B **43** 1993–2006
Troullier N and Martins J L 1991 *Phys. Rev.* B **43** 8861–9
[24] Fuchs M and Scheffler M 1999 *Comput. Phys. Commun.* **119** 67–98
[25] Perdew J P and Wang Y 1992 *Phys. Rev.* B **45** 13244–9
[26] Bader R W 1991 *Chem. Rev.* **91** 893
[27] Ghosez Ph, Cockayne E, Waghmare U V and Rabe K M 1999 *Phys. Rev.* B **60** 836
[28] Zhong W and Vanderbilt D 1995 *Phys. Rev. Lett.* **74** 2587–90